ResearchGate

See discussions, stats, and author profiles for this publication at: https://www.researchgate.net/publication/233984083

Spectroscopic and density functional theory investigation of novel Schiff base complexes

ARTICLE *in* SPECTROCHIMICA ACTA PART A MOLECULAR AND BIOMOLECULAR SPECTROSCOPY · NOVEMBER 2012

Impact Factor: 2.35 · DOI: 10.1016/j.saa.2012.10.058 · Source: PubMed

CITATIONS
11

READS
95

5 AUTHORS, INCLUDING:

Walid M I Hassan
Qatar University
13 PUBLICATIONS **69** CITATIONS
SEE PROFILE

Ehab Mostafa Zayed
National Research Centre, Dokki, 12622 Giz…
24 PUBLICATIONS **116** CITATIONS
SEE PROFILE

Hussein Moustafa
Cairo University-Faculty of Science
27 PUBLICATIONS **92** CITATIONS
SEE PROFILE

Gehad Genidy Mohamed
Cairo University
144 PUBLICATIONS **2,154** CITATIONS
SEE PROFILE

Available from: Walid M I Hassan
Retrieved on: 23 January 2016

Spectrochimica Acta Part A: Molecular and Biomolecular Spectroscopy 103 (2013) 378–387

Contents lists available at SciVerse ScienceDirect

Spectrochimica Acta Part A: Molecular and Biomolecular Spectroscopy

journal homepage: www.elsevier.com/locate/saa

Spectroscopic and density functional theory investigation of novel Schiff base complexes

Walid M.I. Hassan [a], Ehab M. Zayed [b], Asmaa K. Elkholy [a], H. Moustafa [a], Gehad G. Mohamed [a,*]

[a] Chemistry Department, Faculty of Science, Cairo University, 12613 Giza, Egypt
[b] Green Chemistry Department, National Research Centre, Dokki, 12622 Giza, Egypt

HIGHLIGHTS

- Metal complexes of the general formula [ML]·xH_2O (M = Mn(II), Co(II), Ni(II), Cu(II) and Zn(II) (x = 0–2)) and [ML]·nCl (M = Cr(III), Fe(III) and Th(IV) (n = 1–2)) are prepared.
- They are characterized with analytical and spectroscopic techniques (elemental analyses, IR, ^{1}H NMR, magnetic moment, molar conductance, and thermal analyses.
- On the basis of spectral studies, an octahedral geometry was assigned for the complexes.
- Density functional theory at the B3LYP/6-31G* level of theory were used to investigate molecular geometry.

GRAPHICAL ABSTRACT

New metal complexes of novel Schiff base are prepared and characterized based on elemental analyses, IR, ^{1}H NMR, magnetic moment, molar conductance, and thermal analyses techniques. The complexes are formed in 1:1 [Metal]:[Ligand] ratio, are non-electrolytes except Cr(III), Fe(III) and Th(IV) complexes, are electrolytes, coordinated to the metal ions in a uninegative hexadentate manner with $O_2N_2S_2$ donor sites of the etheric O, azomethine N and thiophenolic S atoms and have octahedral geometry. Density Functional Theory at the B3LYP/6-31G* level of theory were used to investigate molecular geometry, Mulliken atomic charges and energetic.

Optimized geometry of anti-conformers of the ligand in the ground state. Bond lengths are given in angstroms and angles are in degrees. Vector in the middle represent the total dipole moment vector.

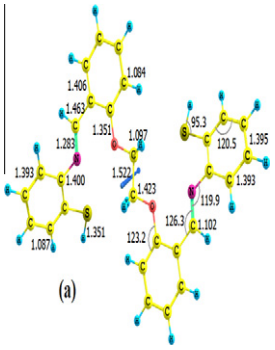

ARTICLE INFO

Article history:
Received 15 September 2012
Received in revised form 19 October 2012
Accepted 25 October 2012
Available online 15 November 2012

Keywords:
Schiff base metal complexes
Bisaldehyde
2-Aminothiophenol
Spectroscopy
Thermal
DFT theoretical investigation

ABSTRACT

Novel Schiff base (H_2L, 1,2-bis[(2-(2-mercaptophenylimino)methyl)phenoxy] ethane) derived from condensation of bisaldehyde and 2-aminothiophenol was prepared in a molar ratio 1:2. The ligand and its metal complexes are fully characterized with analytical and spectroscopic techniques. The metal complexes with Cr(III), Mn(II), Fe(III), Co(II), Ni(II), Cu(II), Zn(II) and Th(IV) have been prepared and characterized by elemental analyses, IR and ^{1}H-NMR spectroscopy, thermal and magnetic measurements. The results suggested that the Schiff base is a bivalent anion with hexadentate OONNSS donors derived from the etheric oxygen (O, O′), azomethine nitrogen (N, N′) and thiophenolic sulphur (S, S′). The formulae of the complexes were found to be [ML]·xH_2O (M = Mn(II) (x = 0), Co(II) (x = 1), Ni(II), (x = 1), Cu(II) (x = 2) and Zn(II) (x = 0)) and [ML]·nCl (M = Cr(III) (n = 1), Fe(III) (n = 1) and Th(IV) (n = 2)). The thermogravimetric analysis of the complexes shows metal oxide remaining as the final product at 700–1000 °C. Density functional theory at the B3LYP/6-31G* level of theory was used to investigate molecular geometry, Mulliken atomic charges and energetics. The synclinal-conformer was found to be responsible for complex formation. The calculation showed that ligand has weak field. Structural deformation and the dihedral angles

* Corresponding author. Tel.: +20 235676896.
E-mail address: ggenidy@hotmail.com (G.G. Mohamed).

1386-1425/$ - see front matter © 2012 Elsevier B.V. All rights reserved.
http://dx.doi.org/10.1016/j.saa.2012.10.058

rotation during complexation were investigated. The binding energy of each complex was calculated. The calculated results are in good agreement with experimental data.

© 2012 Elsevier B.V. All rights reserved.

Introduction

The most important step in the development of metal complexes was perhaps the preparation of a new ligand which exhibit unique properties and novel reactivity. Since, the electron donor and electron acceptor properties of the ligand, structural functional groups and the position of the ligand in the coordination sphere together with the reactivity of coordination compounds may be a factor of different studies [1–11]. Schiff bases are compounds containing an azomethine group (—C═N—), have drawn attention for many years ago. Their metal complexes have been studied, with a variety of transition metal ions, since they frequently exhibit unusual structural properties [12]. These properties have resulted in wide applications in the biological field [13]. Copper(II) complexes are known to be effective against *rheumatoid arthritis* and they also show anti-ulcer activity [14]. This is significant because gastrointestinal irritation often precludes treatment by other anti-arthritic drugs. This is in line with the role of copper in generally preventing gastrointestinal damage by acidic anti-inflammatory agents [15]. Some Schiff base complexes are also used as model molecules for biological oxygen carrier systems [16] as well as having applications in analytical fields [17].

The Schiff base ligands with sulfur and nitrogen donor atoms in their structures, act as good chelating agents for the transition and non transition metal ions [18]. Coordination of such compounds with metal ions such as copper, nickel and iron often enhance their activities [19], as has been reported for pathogenic fungi [20] because of the presence of both hard nitrogen or oxygen and soft sulfur donor atoms in the backbones of these ligands. They readily coordinate with a wide range of transition metal ions yielding stable and intensely colored metal complexes some of which have been shown to exhibit interesting physical and chemical properties [21] and potentially useful biological activities.

In this paper, we have synthesized and characterized a new Schiff base ligand namely 1,2-bis[(3-(4-mercaptophenylimino)methyl)phenoxy] ethane (H_2L) ligand and its di and tri- and tetravalent complex with general formulae $[ML]{\cdot}xH_2O$ (M = Mn(II) ($x = 0$), Co(II) ($x = 1$), Ni(II), ($x = 1$), Cu(II) ($x = 2$) and Zn(II) ($x = 0$)) and $[ML]{\cdot}n$Cl (M = Cr(III) ($n = 1$), Fe(III) ($n = 1$) and Th(IV) ($n = 2$)) via spectral studies, TG and DFT calculations.

Experimental

Materials and reagents

All chemicals used in this study were of the analytical reagent grade and of highest purity available. They included Cu(II) chloride (Sigma), Cr(III), Co(II) and Ni(II) chloride hexahydrates (BDH), Mn(II) chloride (Sigma), ferric chloride hexahydrate (Prolabo), zinc chloride (Ubichem) and thorium chloride (Aldrich). Organic solvents used included absolute ethyl alcohol and dimethylformamide (DMF). These solvents were spectroscopic pure from BDH. De-ionized water collected from all glass equipments was used in all preparations.

Instruments

The molar conductance of solid complexes in DMF (10^{-3} M) was measured using Sybron-Barnsted conductometer (Meter-PM, $E = 3406$). Elemental microanalyses of the separated solid chelates for C, H, N and S were performed in the Microanalytical centers at Cairo University. The analyses were repeated twice to check the accuracy of the data. Infrared spectra were recorded on a Perkin-Elmer FT-IR type 1650 spectrophotometer in the region 4000–400 cm^{-1} as KBr disks. The ^1H NMR spectra were recorded with a JEOL EX-270 MHz in DMSO-d_6 as solvent, where the chemical shifts were determined relative to the solvent peaks. The diffused reflectance spectra were measured on a Shimadzu 3101 pc spectrophotometer. The molar magnetic susceptibility was measured on powdered samples using Faraday method. The diamagnetic corrections were made by Pascal's constant and $Hg[Co(SCN)_4]$ was used as a calibrant. The magnetic data for the background of the sample holder were corrected. The thermal analyses (TG and DTA) were carried out in dynamic nitrogen atmosphere (20 mL min^{-1}) with a heating rate of 10 °C min^{-1} using Shimadzu TG-60H and DTA-60H thermal analyzers.

Synthesis of the H_2L Schiff base

30 mL of ethanolic hot solution (60 °C) of bisaldehyde (3 g, 0.02 mmol) was mixed with hot ethanolic solution (60 °C) of 2-aminothiophenol (5 g, 0.02 mmol) in the same solvent. Then, ethanolic ammonia solution was added to make the medium basic and the reaction mixture was left under reflux for 2 h. The formed solid products were separated by filtration, purified by crystallization from ethanol, washed with diethyl ether and dried in a vacuum over anhydrous calcium chloride. The yellow Schiff base product is produced in 89% yield.

Synthesis of metal complexes

The metal complexes of H_2L was prepared by the addition of hot solution (60 °C) of the appropriate metal chloride (0.664 mmol) in absolute ethanol (15 mL) to the hot solution (60 °C) of the organic ligand (0.3 g HL, 0.664 mmol) in ethanol and DMF (15 ml). The resulting mixture was heated with stirring to evaporate all the solvents to get precipitate. The precipitate was dried and weighed to calculate the yield. All the above steps were repeated for all the selected *d*-transition metals.

Method of calculations

The molecular geometry for all complexes and ligand were fully optimized at the 6-31G(d) basis set (except for thorium complex where SDDALL Basis set were used which impose Stuttgart/Dresden Effective core potential [22]) using Becke's three-parameter-hybrid (B3LYP) method [23–25]. The effect of multiplicity has been tested and the energetic shown here is for the most stable one. The B3LYP method provides energetic typically better than Hartree–Fock method [26] and can reproduce better geometrical parameters comparable to the experimental values than any other method [27]. All the geometry optimization calculations were done using the Gaussian 09 software package [28]. The optimized structures were visualized using Chemcraft version 1.6 package [29]. The geometry optimization of all ligand conformers and metal complexes follows C_2 point group which make all atoms and their structural and energetic parameters are symmetrical around a twofold axis passing by the center of aliphatic ethylene bond.

Results and discussion

Mass spectrum of the new Schiff base ligand

The electron impact spectrum of the newly prepared H_2L ligand is recorded and investigated at 70 eV of electron energy. The mass spectrum of the studied Schiff base (Fig. 1) is characterized by moderate to high relative intensity molecular ion peaks. It is obvious that, the molecular ion peaks are in good agreement with its suggested empirical formula as indicated from elemental analyses (Table 1). The mass spectrum of H_2L shows a well defined parent peak at m/z 484 (M^+) with a relative intensity = 1%. The parent ion and the fragments obtained by cleavage in different positions in H_2L molecule are shown in Scheme 1.

Characterization of metal complexes

Metal complexes were obtained upon reaction between metal ions and H_2L ligand at 1:1 M:L ratio. The synthesized azo-Schiff base ligand and its complexes are very stable at room temperature in the solid state. The ligand is insoluble in common organic solvents on cold. The ligand and its metals complexes are generally soluble in DMF and DMSO. The yields, melting/decomposition points, elemental analyses, of L and its metals complexes are presented in Table 1. The analytical data are in a good agreement with the proposed stoichiometry of the complexes. The ligand decomposed at temperatures higher than 100 °C, while all complexes decomposed at temperatures higher than 300 °C.

^{1}H-NMR

The ^{1}H-NMR data of H_2L ligand (Fig. 2a) and its Zn(II) complex (Fig. 2b), recorded in DMSO-d_6, show a sharp band at 8.4 and 8.5 ppm which may be assigned to the azomethine protons (—CH═N, 1H), respectively. The SH signal which appears in the free ligand at 5.2 ppm, completely disappeared in the Zn complex indicating that the SH proton is removed during chelation process. However, a singlet and multiple bands at 4.9 and 6.4–8 ppm may be attributed to methylene and the aromatic protons in the free H_2L ligand. The resonance signals obtained for Zn(II) complex show down field shift as compared to the corresponding ligand indicating the coordination of ligand to Zn(II) ion.

Molar conductance measurements

Conductivity measurements in non-aqueous solutions have frequently been used in structural studies of metal chelates within the limits of their solubility. They provide a method of testing the degree of ionization of the complexes, the molar ions that a complex liberates in solution, the higher will be its molar conductivity and vice versa. The non-ionized complexes have negligible value of molar conductance. The molar conductivities of 10^{-3} molar solutions of the metal chelates at 25 ± 2 °C are measured and the data obtained are listed in Table 1. It is concluded from these results that Co(II), Ni(II), Cu(II), Mn(II) and Zn(II) complexes with H_2L ligand are considered as non electrolytes. These low molar conductance values indicate their non ionic nature. In addition Cr(III) and Fe(III)-H_2L complexes have molar conductance values of 74 and 88 Ω^{-1} mol^{-1} cm^2, respectively, indicating their ionic nature and they are considered as 1:1 electrolytes. The Th(IV) complex has molar conductance value of 180 Ω^{-1} mol^{-1} cm^2 (Table 1) indicating its ionic nature and it is considered as 1:2 electrolyte.

IR Spectra and mode of bonding

The IR data of H_2L Schiff base ligand and its complexes are listed in Table 2. The IR spectra of the complexes are compared with those of the free ligand. In order to determine the coordination sites that may be involved in chelation, spectrum of the ligand is of good help for achieving this goal. The shift in position and/or the intensities of these guide peaks. These guide peaks are listed in Table 2.

The $\upsilon(C–S)_{Sym}$, $\upsilon(C–S)_{asym}$ and $\upsilon(S–H)$ stretching vibrations are observed at 749, 800 and 2356 cm^{-1} in the free ligand, respectively. The band due to $\upsilon(S–H)$ is disappeared in the complexes indicating the participation of the thiol sulfur in deprotonated form. The participation of the thiol sulfur atom in the complex formation is further evidenced from the shift in position of the symmetric and asymmetric bands to 749–752 and 810–814 cm^{-1}, respectively. It was found that $\upsilon(CH═N)$ of the azomethine stretching vibration is found in the free ligand at 1601 cm^{-1} [30–33]. This

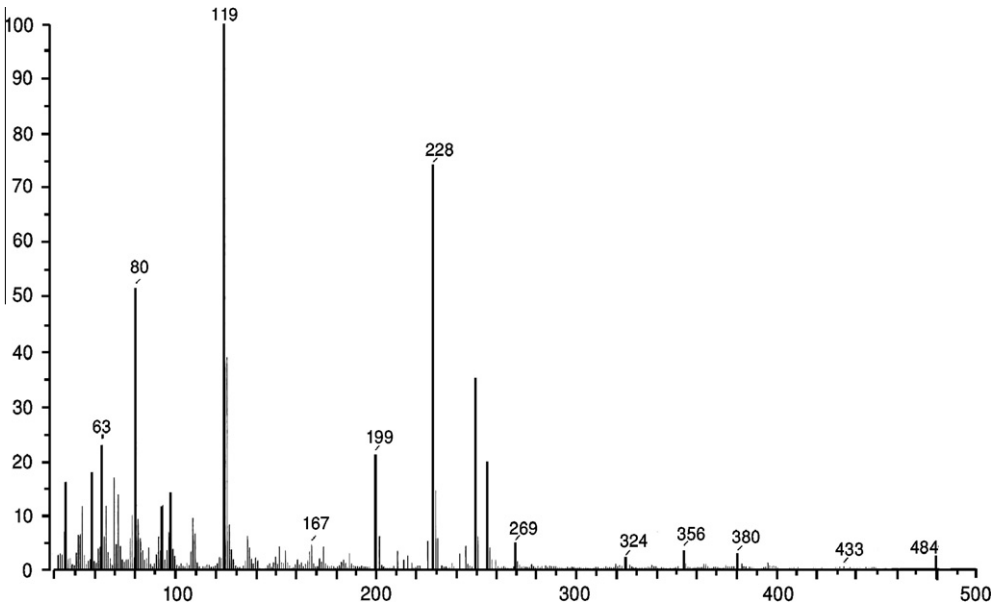

Fig. 1. Mass spectrum of the Schiff base ligand.

Table 1
Analytical and physical data of H_2L Schiff base ligand and its complexes.

Compound	Color (% yield)	Melting point (°C)	% Found (calcd.)					μ_{eff} (B.M.)	A_m (Ω^{-1} mol^{-1} cm^2)
			C	H	N	S	M		
H_2L	Reddish brown	100	69.42	4.96	5.79	13.22	–		
($C_{28}H_{24}N_2O_2S_2$)	(89)		(69.20)	(4.27)	(5.67)	(13.10)			
[CrL]Cl	Green	>300	59.01	3.86	4.92	11.24	9.11	4.2	38.0
$C_{28}H_{22}ClCrN_2O_2S_2$	(78)		(58.80)	(3.40)	(4.60)	(11.30)	(9.21)		
[MnL]	Dark green	>300	61.58	4.17	5.21	11.92	10.23	5.7	32.0
$C_{28}H_{22}MnN_2O_2S_2$	(74)		(61.70)	(4.20)	(4.90)	(11.63)	(10.43)		
[FeL]Cl	Brown	>300	57.60	3.84	4.88	11.16	9.74	5.6	88.0
$C_{28}H_{22}ClFeN_2O_2S_2$	(69)		(57.70)	(3.60)	(4.50)	(10.90)	(9.63)		
[CoL]·H_2O	Black	>300	61.90	3.90	5.20	11.82	11.00	4.3	40.0
$C_{28}H_{22}CoN_2O_2S_2$	(72)		(61.88)	(4.05)	(5.16)	(11.79)	(10.87)		
[NiL]·H_2O	Green	>300	62.16	4.07	5.18	11.84	10.82	3.1	34.0
$C_{28}H_{24}NiN_2O_3S_2$	(68)		(61.90)	(3.9)	(5.33)	(11.49)	(10.64)		
[CuL]·2H_2O	Brown	>300	61.59	4.03	5.13	11.73	11.64	1.8	30.0
$C_{28}H_{26}CuN_2O_4S_2$	(73)		(61.20)	(4.16)	(5.32)	(11.52)	(11.52)		
[ZnL]	Yellowish brown	>300	61.38	4.02	5.12	11.69	11.95	Diamagnetic	25.0
$C_{28}H_{22}N_2O_2S_2Zn$	(75)		(61.02)	(3.80)	(5.02)	(11.39)	(11.86)		
[ThL]Cl_2	Black	>300	42.81	2.80	3.67	8.15	29.56	Diamagnetic	180.0
$C_{28}H_{22}Cl_2N_2O_2S_2Th$	(67)		(42.53)	(2.60)	(3.50)	(7.90)	(29.43)		

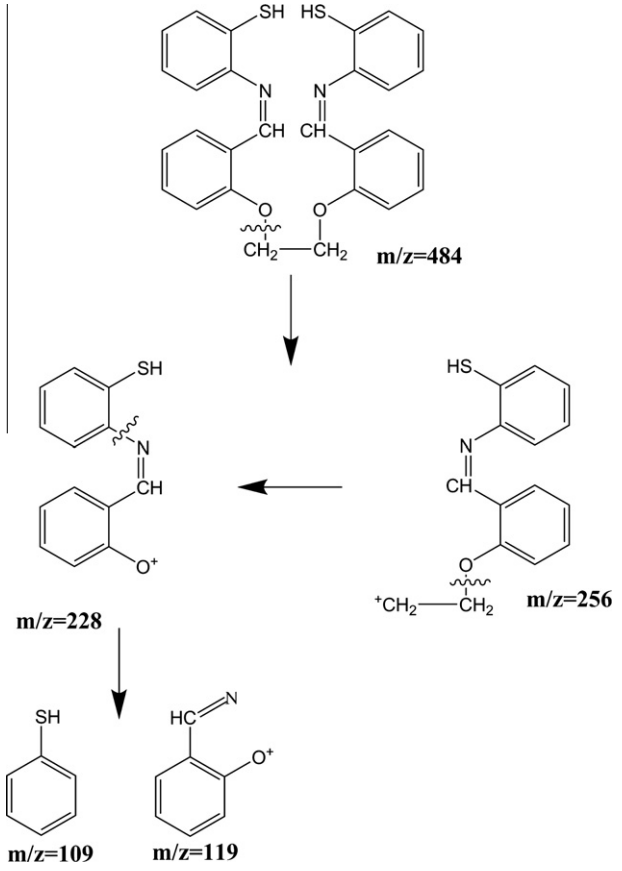

Scheme 1. Mass fragmentation pattern of H_2L ligand.

band is shifted to lower wave number at 1585–1597 cm^{-1} in the complex indicating the participation of the azomethine nitrogen in coordination (M–N).

The IR spectra of the complexes clearly demonstrated that the COC stretching vibration is altered compared to ligand due to conformational changes. The fact that the C—O—C absorption of the complexes is shifted to lower wave numbers 1026–1030 cm^{-1} in the complexes compared to that of the ligand (1028 cm^{-1}) also confirms the complex formation [30–33].

New bands are found in the spectra of complexes in the regions 525–563, 455–459 and 428–438 cm^{-1} which are assigned to υ(M–O), υ(M–N), and υ(M–S) stretching vibrations, respectively. Therefore, from the IR spectra it is concluded that H_2L Schiff base is binegative hexadentate ligand with NNOOSS coordination sites and binds to the metal ions through azomethine N, ether O, and deprotonated thiol S.

Solid reflectance and magnetism

The observed magnetic moment of [CrL]Cl chelate is found to be 4.2 B.M which indicates the presence of this complex in octahedral geometry. The diffused reflectance spectrum of this complex exhibits bands at 13,793, 17,542 and 28,208 cm^{-1}. These bands are assigned to $^4A_{2g}(F) \rightarrow 4T_{2g}(F)$, $^4A_{2g}(F) \rightarrow 4T_{2g}$ and $^4A_{2g}(F) \rightarrow 4T_{2g}(P)$ spin allowed *d–d* transitions, respectively. These bands suggest an octahedral geometry for the Cr(III) complex [34–37].

The diffused reflectance spectrum of the [MnL] complex shows three bands at 17,361, 22,446 and 26,809 cm^{-1} which are assignable to $^6A_{1g} \rightarrow {}^4T_{1g}$, $^6A_{1g} \rightarrow {}^4T_{2g}(G)$ and $^6A_{1g} \rightarrow {}^4T_{1g}(D)$ transitions, respectively. The magnetic moment value is found to be 5.7 B.M, which indicates that the complex has octahedral geometry [34,38–40].

From the diffused reflectance spectrum and according to previously published data [18,22,23], it has been observed that, the [FeL]Cl chelate exhibits bands at 16,652, 17,547 and 21,905 cm^{-1}. These bands can be assigned to the $^6A_{1g} \rightarrow T_{2g}(G)$, $^6A_{1g} \rightarrow {}^5T_1g$ and $^6T_{1g} \rightarrow {}^5T_1g$ (D) transitions in octahedral geometry of the complex. The observed magnetic moment value of Fe(III) complex is found to be 5.6 B.M, indicating octahedral geometry [34,39–41]. The spectrum shows also band at 28,368 cm^{-1} which may be attributed to ligand to metal charge transfer.

The magnetic moment value of the [CoL]·H_2O complex is found to be 4.3 B.M, indicating octahedral geometry [34,36–39]. The diffused reflectance spectrum gives three bands at 12,787, 16,420 and 22,274 cm^{-1}. The bands observed are assigned to the transitions $^4T_{1g}(F) \rightarrow 4T_{2g}(F)$ (ν_1), $^4T_{1g}(F) \rightarrow 4A_{2g}(F)$ (ν_2) and $^4T_{1g}(F) \rightarrow 4T_{1g}(P)$ (ν_3), suggesting the existence of this complex in an octahedral geometry.

The studied [NiL]·H_2O complex is high spin with a room temperature magnetic moment value of 3.1 B.M., which is in the normal range observed for octahedral Ni(II) complexes (μ_{eff} = 2.9–3.7 B.M.) [34–38]. The diffused reflectance spectrum displays three bands at ν_1: (12,190) cm^{-1}: $^3A_{2g}(F) \rightarrow {}^3T_{2g}(F)$, ν_2: (17,050) cm^{-1}:

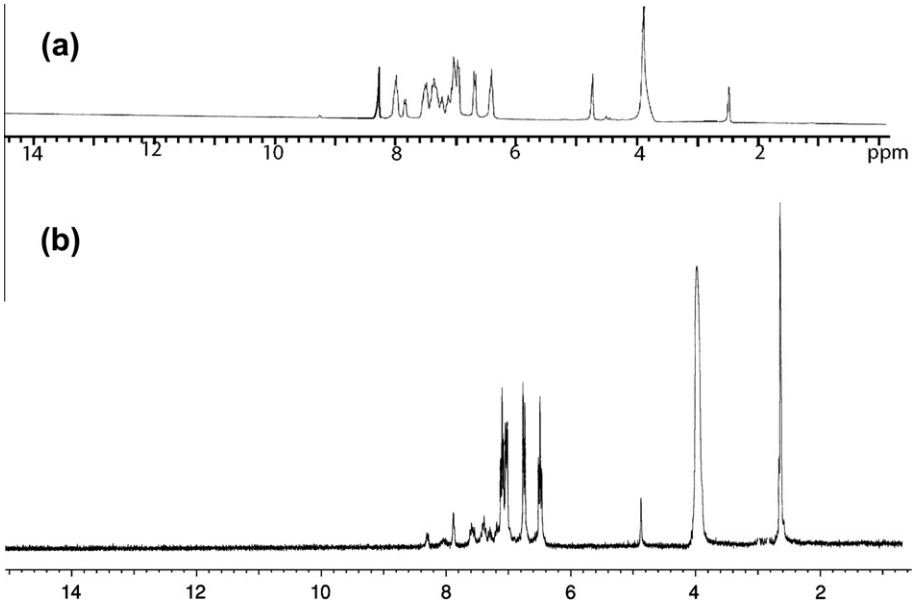

Fig. 2. The ^{1}H-NMR spectral chart of (a) H_2L ligand and (b) Zn(II) complex.

Table 2
IR data (4000–400 cm^{-1}) of H_2L Schiff base ligand and its metal complexes.

	υ(CH=N)	υ(S—H)	υ_{Sym} (C—S)	υ_{asym} (C—S)	υ(C—O—C)	υ(M—O)	υ(M—N)	υ(M—S)
H_2L	1601sh	2356sh	749w	800w	1028s	–	–	–
[CrL]Cl	1589s	Disappear	755sh	810w	1026m	559w	459w	428w
[MnL]	1585m	Disappear	752sh	810w	1026m	525w	455w	424w
[FeL]Cl	1589m	Disappear	752sh	814w	1030m	563w	455m	428m
[CoL]·H_2O	1589sh	Disappear	752s	810w	1030m	525w	455w	428w
[NiL]·H_2O	1589sh	Disappear	752s	810w	1030m	559w	459w	428w
[CuL]·$2H_2O$	1597m	Disappear	752sh	810w	1030m	535w	459w	428w
[ZnL]	1590m	Disappear	752sh	810w	1030m	530w	455w	428w
[ThL]Cl_2	1589m	Disappear	752sh	814w	1030m	529w	455w	424w

s: Strong, m: medium, w: weak, sh: sharp.

$^3A_{2g}(F) \rightarrow {}^3T_{1g}$ (F) and ν_3: (21,321) cm^{-1}: $^3A_{2g} \rightarrow {}^3T_{1g}$ [40,41]. The spectrum shows also a band at 29,197 cm^{-1}, which may be attributed to ligand to metal charge transfer.

The reflectance spectrum of the [CuL]·$2H_2O$ chelate shows allow intensity band at 18,484 cm^{-1}. This can be attributed to $^2B_{1g} \rightarrow {}^2A_{1g}$ transition. The ^2E_g and $^2T_{2g}$ states of the octahedral Cu(II) ion split under the influence of the tetragonal distortion and can be such as to cause the transitions $^2B_{1g} \rightarrow {}^2B_{2g}$ and $^2B_{1g} \rightarrow {}^2E_g$ to remain unresolved in the spectrum of the complex. In a similar fashion [34–39] the magnetic moment of this complex was measured and has been found equal to 1.8 B.M, which falls within the range normally observed for octahedral Cu(II) complexes. A moderately intense peak observed in the range of 26,737 cm^{-1} is due to ligand to metal charge transfer [41].

The Zn(II) and Th(IV) complexes are diamagnetic (Table 1) and according to the empirical formulae an octahedral geometry was proposed for these complexes.

Thermal analysis (TG, DTG and DTA)

Thermal analyses (TG, DTG and DTA) of the Schiff base ligand (H_2L) and its chelates are used to: (i) get information about the thermal stability of these new complexes, (ii) decide whether the water molecules, if present, are inside or outside the inner coordination sphere of the central metal ion, and (iii) suggest a general scheme for thermal decomposition of these chelates. The TG (and DTG) and DTA data are listed in Table 3. The weight losses for each chelate are calculated within the corresponding temperature ranges.

The TG curve of Schiff base H_2L, exhibits a first estimated mass loss of 21.94% (calcd. 21.48%) at 100–300 °C, which may be attributed to loss of C_7H_4O molecule. In the second stage within the temperature range 300–400 °C with a mass loss of 10.99% (calcd. 11.98%) can be attributed to the liberation of CO and NO molecules as gases. The third stage within the temperature range 400–550 °C with estimated mass loss 16.92% (calcd. 17.76%) can be assigned to the loss of C_3H_4NS molecule (Table 3). The fourth stage within the temperature range 550–1000 °C with estimated mass loss of 52.19% (calcd. 52.01%) can be attributed to loss of $C_{17}H_{16}S$ molecule. These steps have total mass losses of 100% (calcd. 100%). These loses appear in the DTA curves as two exothermic peaks at 530 and 790 °C.

The TG data of Cr(III) chelate are listed in Table 3. The complex decomposes into two stages within the temperature range from 50 to 850 °C. The first step corresponds to the loss of $C_{20}H_{16}NS_2$ molecule in the temperature range 50–300 °C with estimated mass loss 61.58% (calcd. 62.32%). The second step corresponds to the loss of C_8H_8NO molecule in the temperature range from 300 to 850 °C with estimated mass loss 26.16% (calcd. 25.00%). The total mass loss of the decomposition steps is found to be 87.74% (calcd.

Table 3
Thermal analysis data of H_2L Schiff base ligand and its metal complexes.

Compound	TG range (°C)	DTG_{Max} (°C)	n^*	Mass loss calcd. (Est.%)	Total mass loss%	Assignment	Metallic residue	DTA (°C)
H_2L	100–300	250	1	21.48 (21.94)	100	Loss of C_7H_4O	–	
	300–400	350	1	11.98 (10.99)	(100.0)	Loss of CO and NO	–	530(−), 790(+)
	400–550	510	1	17.76 (16.92)		Loss of C_3H_4NS	–	
	550–1000	590	1	52.01 (52.19)		Loss of $C_{17}H_{16}S$	–	
[Cr(L)]Cl	50–300	270	1	62.32 (61.58)	87.32	Loss of $C_{20}H_{16}NS_2$	CrO	
	300–850	470	1	25.00 (26.16)	(87.74)	Loss of C_8H_8NO		333(+), 730(+)
[Mn(L)]	150–400	300	1	74.21 (76.65)	94.8	Loss of $C_{24}H_{18}N_2S_2$	MnO	
	400–700	550	1	16.14 (16.75)	(93.40)	Loss of C_2H_4O		187(−), 398(−)
[Fe(L)]Cl	50–390	210, 270	2	36.62(38.05)	75.49	Loss of $C_{13}H_9NS$	FeO	
	390–750	550	1	37.14(37.22)	(75.47)	Loss of $C_{13}H_9NOS$	+2C	320(+), 560(−)
	750–1000	870	1	1.73(0.20)		Loss of C_2H_4Cl		
[Co(L)]·H_2O	30–100	50	1	3.20 (3.32)	86.29	Loss of H_2O	CoO	
	100–270	120	1	6.06 (4.94)	(83.50)	Loss of H_2S		77(−), 124(−),
	270–420	300	1	16.05 (15.38)		Loss of C_7H_6		254(+), 276(+), 302(+)
	420–700	510	1	60.98 (59.88)		Loss of $C_{21}H_{14}N_2OS$		
[Ni(L)]·H_2O	30–100	50	1	3.21 (3.07)	80.26	Loss of H_2O	NiO	
	100–400	250	1	24.78 (32.013)	(78.06)	Loss of $C_{13}H_9NO$	+3C	376(−), 795(−), 800(+)
	400–1000	550	1	42.27 (42.89)		Loss of $C_{12}H_{15}NS_2$		
[Cu(L)]·$2H_2O$	50–200	150	1	6.16 (6.60)	86.63	Loss of $2H_2O$	CuO	
	200–400	305	1	43.83 (43.67)	(85.06)	Loss of $C_{15}H_{14}NOS$		157(+), 331(−)
	400–800	630, 880	2	36.33 (35.79)		Loss of $C_{13}H_{10}NS$		
[Th(L)]·Cl_2	50–400	330	1	25.14 (25.59)	66.7	Loss of $C_{13}H_9N$	ThO	
	400–600	500	1	24.72 (26.14)	(73.31)	Due to loss of C_9H_7NOS		204(−), 586(+), 659(+)
	600–1000	800	1	16.00 (21.11)		Due to loss of C_5H_6S		

n^* = Number of decomposition steps. (−) = exothermic peak, (+) = endothermic peak.

87.32%). It is clear from these data that these mass losses are accompanied by two endothermic peaks at 333 and 730 °C.

The thermogram of Mn(II) chelate shows two decomposition steps. The first step of decomposition occurs within the temperature range of 150–400 °C and corresponds to the loss of $C_{24}H_{20}N_2S_2$ molecule with a mass loss 74.21% (calcd. 76.85%). The subsequent step within the temperature range 400–700 °C corresponds to removal of C_2H_4O molecule with a mass loss 16.75% (calcd. 16.14%) leaving the metal oxide as residue. The overall weight loss amounts to 94.80% (calcd. 93.40%). The DTA data are listed in Table 3. It is clear from these date that these mass losses are accompanied by two exothermic peaks at 187 and 398 °C.

The data of thermal decomposition of Fe(III) chelate are given in Table 3. The first stage within the temperature range 50–390 °C with mass loss 38.05% (calcd. 36.62%) corresponds to the loss of $C_{13}H_9NS$ molecule. The second step occurs within the temperature range 390–750 °C with mass loss 37.22% (calcd. 37.14%) and corresponds to the loss of $C_{13}H_9NOS$ molecule. The third step within the temperature range 750–1000 °C with mass loss 36.62% (calcd. 38.05%) may be due to loss of C_2H_4Cl molecule. The overall weight loss amounts to be 75.47% (calcd. 75.49%). These mass losses are accompanied by exothermic peak at 560 °C and endothermic peaks at 320 °C

The Co(II) chelate (Table 3) decomposes in four steps within the temperature range from 30 to 700 °C. The first step is attributed to the loss of hydrated water molecule with mass loss 3.32% (calc. 3.20%). The second step occurs within the temperature range 100–270 °C and can be assigned to loss of H_2S gas with mass loss 4.94% (calcd. 6.06%). The third step within the temperature range 270–420 °C corresponds to loss of C_7H_6 molecule with mass loss of 15.38% (calcd. 16.06%). The final step is due to removal of $C_{21}H_{14}N_2OS$ molecule with mass loss of 59.88% (calcd. 60.98%) leaving CoO as residue. The overall weight loss amounts to 83.52% (calcd. 86.29%). These steps are accompanied by endothermic peaks at 245, 276 and 302 °C and two exothermic peaks at 77 and 124 °C.

The TG curve of the Ni(II) chelate shows three stages of decomposition within the temperature range 30–1000 °C. The first stage of decomposition within the temperature range 30–100 °C corresponds to the loss of water of hydration with mass loss 3.07% (calcd. 3.21%). The second step within the temperature range 200–400 °C involves the loss of $C_{13}H_9NO$ molecule with mass loss of 32.01% (calcd. 34.78%). The last step within the temperature range 400–1000 °C involves loss of $C_{12}H_{15}NS_2$ molecule with mass loss 42.89% (calcd. 42.27%). The overall weight loss is 78.06% (calcd. 80.26%). These steps are accompanied by exothermic peaks at 376 and 795 °C and one endothermic peak at 800 °C.

On the other hand, Cu(II) chelate exhibits four decomposition steps as shown in Table 3. The first step within the temperature range 50–200 °C corresponds to the loss of hydrated water with estimated mass loss 6.60% (calcd. 6.16%). The second step occurs in the temperature range 200–400 °C and corresponds to the loss of $C_{15}H_{14}NOS$ molecule with mass loss 43.67% (calcd. 43.83%). The final step is due to the loss of $C_{13}H_{10}NS$ molecule in the temperature range 400–800 °C with mass loss 35.79% (calcd 36.33%). The total mass losses of the decomposition steps are found to be 85.06% (calcd. 86.36%) leaving CuO as a residue. DTA data (listed in Table 3 reveal that these mass losses are accompanied by one exothermic peak at 331 °C and one endothermic peak at 157 °C.

The TG data of Th(IV) chelate are listed in Table 3. It decomposes in three stages within the temperature range 50–1000 °C. Within the temperature range from 50 to 400 °C, the first step corresponds to the removal of $C_{13}H_9N$ molecule with mass loss 25.59% (calcd. 25.14%). The second step from 400 to 600 °C can be assigned to the loss of C_9H_7NOS molecule with mass loss 26.14% (calcd 24.72%). The final step in the temperature range 600–1000 °C corresponds to the loss of C_5H_6S molecule with mass loss 21.11% (calcd. 16.00%). The total mass losses of the decomposition steps are found to be 73.31% (calcd 66.70%). It's clear from these data that these mass losses are accompanied by one exothermic peak at 204 °C and endothermic peaks at 586, 659 °C.

Theoretical investigation

Geometry and energetic of the ligand

The optimized geometry of the H_2L ligand is shown in Fig. 3. The anti-conformer ligand structure (Fig. 3a) is almost planar with thiophenol ring which has dihedral angle 40° out of the molecular

plane of the phenol in the ground state. The two oxygen atoms occupy anti-conformer in the global minimum conformer with dihedral angle of 179.7°. The chelation process involves rotation around aliphatic CH_2 groups from the anti-conformer to synclinal-conformer. The synclinal-conformer shown in Fig. 3b plays an important role in the chelation process. In the synclinal-conformer the two oxygen atoms has dihedral angle of −80.3°. The bond lengths and bond angle of both anti and synclinal-conformers are very similar with exception of the rotation around the aliphatic C—C bond.

The S—H bond length of the ligand is 1.351 Å which is in good agreement with calculated S—H bond lengths of substituted thiophenol [42]. The optimized geometry of the deprotonated ligand (L^{2-}) in the anti- and synclinal-conformers is shown in Fig. 4. The geometry of L^{2-} and H_2L are very similar with slight change on some bond angles. The C—S bond length in L^{2-} is slightly smaller than in H_2L which indicates a stronger bond between the S atom and thiophenol ring in case of L^{2-} compared to the H_2L.

The energetic parameters for the H_2L and L^{2-} forms of the ligand are summarized in Table 4. The synclinal-conformer is less stable than the anti-conformer by 1.68 and 2.06 kcal/mol for H_2L and L^{2-}, respectively. The energy difference ΔE between LUMO (lowest unoccupied molecular orbital) and HOMO (highest occupied molecular orbital) is smaller in case of L^{2-} ligand than that of the H_2L ligand itself. The lower ΔE the higher the reactivity, this indicates that L^{2-} is more reactive than the H_2L.

The Mulliken atomic charges are almost the same on O atoms in both L^{2-} and H_2L but vary on both N and S atoms. The summation of all charges on the six donating atoms (donor charge) is shown in Table 4. The donor charge is maximum in case of synclinal-conformer of L^{2-}. The charge on all atoms other than donating atoms on ligand is shown as (remaining) in Table 4. The dipole moment for synclinal-conformer of L^{2-} is 4.147 Debye which is higher than dipole moment of all other conformers. The higher dipole moment usually indicates higher polarity and higher tendency to react with other charged compounds [43].

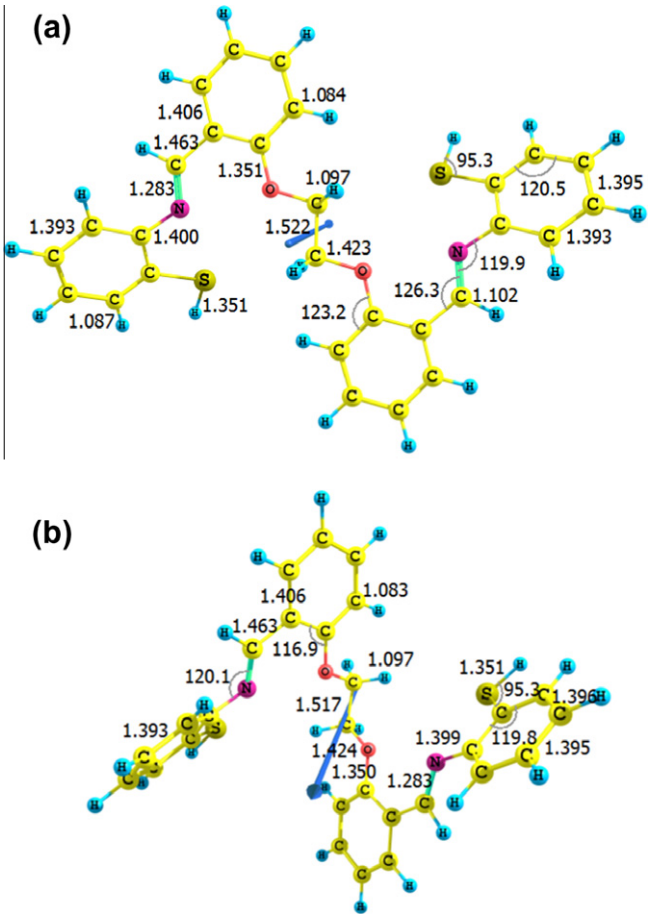

Fig. 3. Optimized geometry of (a) anti- and (b) synclinal-conformers of the ligand in the ground state. Bond lengths are given in angstroms and angles are in degrees. Vector in the middle represent the total dipole moment vector.

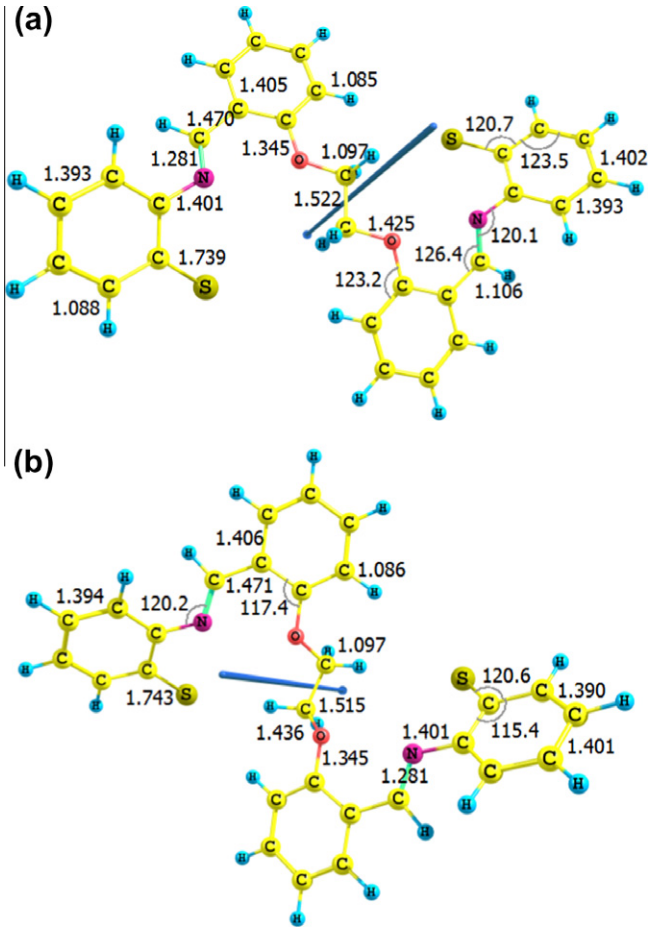

Fig. 4. Optimized geometry of (a) anti- and (b) synclinal-conformers of the L^{2-} in the ground state. Bond lengths are given in angstroms and angles are in degrees. Vector in the middle represent the total dipole moment vector.

Structural parameter for the complexes

From the experimental sections, we have established the ratio of M:L using molar conductance. The expected geometry is octahedral complex as indicated from solid reflectance and magnetism. The ligating centers are O, O′, N, N′, S and S′ atoms shown in Fig. 5. The S and S′ occupy the axial positions while O, N and O′,

Table 4
The energetic, and Mulliken atomic charges of H_2L, L^{2-} and their anti- and synclinal-conformers.

	H_2L (anti)	H_2L (synclinal)	L^{2-}(anti)	L^{2-}(synclinal)
E_{total}, a.u.	−2137.7171	−2137.7144	−2136.5509	−2136.5476
E_{LUMO}, eV	−1.5187	−1.4335	3.5966	3.6940
E_{HOMO}, eV	−5.4815	−5.3827	1.2340	1.2653
ΔE, eV	3.9628	3.9492	2.3626	2.4287
O-charge	−0.494855	−0.485614	−0.480414	−0.485846
N-charge	−0.458655	−0.455356	−0.386328	−0.386123
S-charge	−0.003936	−0.007373	−0.556362	−0.561443
Donors-charge	−1.91489	−1.896686	−2.84621	−2.866824
Remaining	+1.91489	+1.896686	+0.84621	+0.866824
μ (debye)	0.7669	0.0015	3.1993	4.147

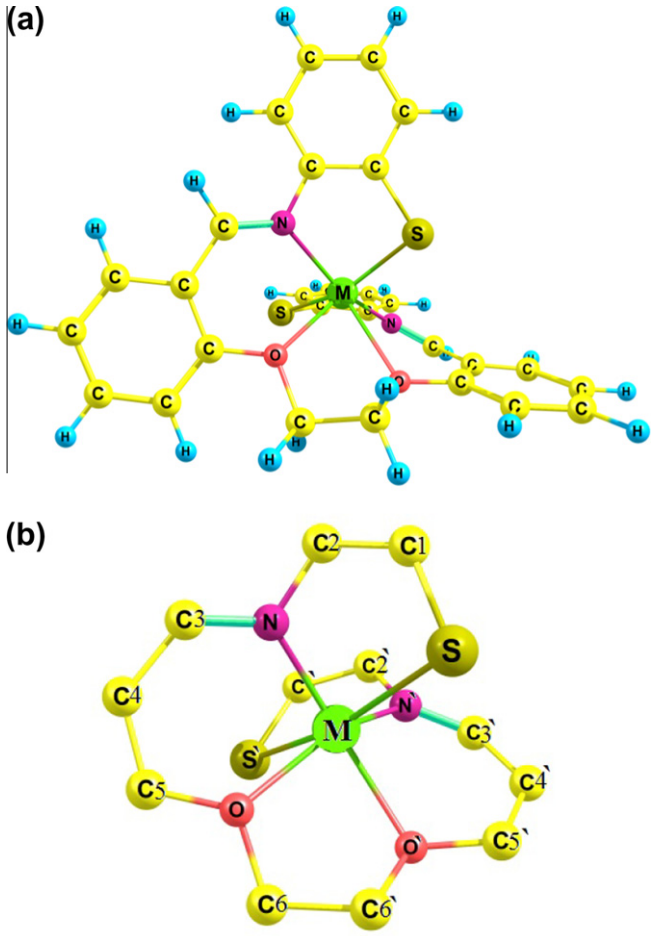

Fig. 5. (a) Ground state optimized geometry of the complex where M is the metal atom. (b) Atom numbering.

N′ occupy the equatorial positions. The numbering used (shown in Fig. 5b) is designed according to C_2 point group. The C_2 point group gives identical structural parameter and charges on each atom (O, N, S, C1–C6) and its atom dash (O′, N′, S′, C1′–C6′), respectively.

The calculated optimized geometry using B3LYP/6-31G(d) method for all metal complexes is shown in Fig. 5a and Table 5. The studied complexes in this work fall into three main groups: The first group includes divalent metal complexes of Mn(II), Co(II), Ni(II), Cu(II) and Zn(II). The second group includes trivalent metal complexes of Cr(III) and Fe(III). The third group includes metal complex with tetravalent Th(IV) metal.

Divalent metal complexes. The C1—C2, C3—C4, C4—C5 and C6—C6′ bond lengths have slight changes during complexation process in the range of 0.02 Å. This indicates the effect of complex on geometrical parameters which are localized mainly near to the ligating atoms. The M—N and M—O bond lengths decrease as we go from Mn to Cu across 3d period. The M—N and M—O bond lengths are slightly longer in case of Zn complex than Mn complex. The M—S bond length varies drastically from metal complex to another. The M—S bond length is longest in case of Cu complex and shortest in case of Zn complex with a difference of 0.39 Å (16%). The S—C1, N—C2, N—C3 and O—C5 bond lengths of divalent complexes show a general trend of slightly elongation compared to synclinal L^{2-}. The O—C5 bond length is shortest in case of Co and Zn complexes (2.3% compared to ligand) and longest in case of Cu complex (2.9% compared to ligand). The maximum variation in bond length is further decease from 1.3% for N—C2 and S—C1 to 0.7% in case of N—C3.

The calculated bond angles of the studied complexes vary as shown in Table 5. In regular octahedral complexes SMS′ and NMO′ bond angles are expected to be 180°. SMS′ bond angle approaches regular octahedral for Ni complex with angle around 169° while maximum deviation is calculated for Co complex with angle 149°. NMO′ bond angles is far away from regular octahedral in all divalent complexes since it ranges from 127° in Co complex to 155° in Cu complex. The calculated bond angels suggested distorted octahedral complexes.

The dihedral angle NC3C4C5 jumps from 2.7° in case of L^{2-} synclinal-conformer to a range from 24.8° to 27.7° in case of Cu and Zn complexes, respectively. The dihedral angle OC6C6′O′ change from −88.5 in case of L^{2-} synclinal-conformer to a range from −61.9° to

Table 5
Structural parameter calculated for Schiff base ligand and its metal complexes.

	H_2L(anti)	H_2L(synclinal)	L^{2-}(anti)	L^{2-}(synclinal)	[Mn(L)]	[Co(L)]·H_2O	[Ni(L)]·H_2O	[Cu(L)]·$2H_2O$	[Zn(L)]	[Cr(L)]Cl	[Fe(L(]Cl	[Th(L)].Cl_2
C1—C2	1.413	1.413	1.440	1.439	1.420	1.418	1.416	1.419	1.419	1.408	1.413	1.413
C3—C4	1.463	1.463	1.470	1.471	1.464	1.459	1.462	1.461	1.463	1.454	1.453	1.457
C4—C5	1.423	1.423	1.425	1.424	1.414	1.412	1.415	1.414	1.414	1.414	1.413	1.416
C6—C6′	1.522	1.516	1.522	1.515	1.511	1.509	1.513	1.514	1.510	1.511	1.507	1.516
M—N					2.303	2.226	2.024	1.976	2.307	2.028	2.184	2.553
M—O					2.445	2.441	2.238	2.154	2.490	2.128	2.286	2.472
M—S					2.472	2.355	2.477	2.716	2.326	2.401	2.357	2.676
S—C1	1.787	1.787	1.739	1.743	1.766	1.758	1.760	1.751	1.764	1.776	1.764	1.855
N—C2	1.400	1.399	1.401	1.401	1.418	1.420	1.419	1.415	1.413	1.430	1.419	1.441
N—C3	1.283	1.283	1.281	1.281	1.287	1.290	1.287	1.288	1.285	1.292	1.293	1.312
O—C5	1.351	1.340	1.345	1.345	1.381	1.376	1.384	1.385	1.376	1.406	1.392	1.444
O—C6	1.423	1.424	1.425	1.436	1.431	1.427	1.433	1.435	1.427	1.451	1.441	1.501
∠SMO					113.4	120.9	103.7	103.936	115.6	103.8	117.1	139.7
∠SMO′					85.1	86.3	84.7	85.478	85.8	86.0	85.6	107.8
∠SMN					78.4	81.7	79.8	76.5	80.1	79.8	79.9	73.5
∠SMO′					96.1	91.7	94.6	96.6	94.1	92.7	90.4	115.1
∠SMS′					157.0	148.5	169.2	167.9	154.1	172.1	152.7	101.5
∠OMO					69.6	67.10	78.5	80.0	68.1	81.3	73.2	64.5
∠NMN′					152.3	155.7	118.4	111.4	157.2	109.2	138.3	167.3
∠NMO					74.8	75.1	84.2	87.6	73.2	86.9	79.6	69.4
∠NMO′					130.1	127.3	153.4	154.1	128.1	158.9	138.8	99.5
∠NC3C4C5	−1.9	−6.4	6.1	2.7	27.5	25.5	25.5	24.8	27.7	21.8	22.2	23.0
∠OC6C6′O′	−179.7	−80.4	−176.6	−88.5	−64.5	−61.9	−64.1	−62.2	−65.2	−57.7	−59.1	−48.2
∠SC1C2N	−2.1	−2.2	−7.2	−6.6	0.2	2.0	−0.8	−1.5	0.4	2.3	0.9	2.2
∠C3C4C5O	−0.3	−2.1	0.2	−5.0	3.8	3.1	3.4	3.7	3.7	2.6	5.4	−3.8

−65.2° in case of Co and Zn complexes, respectively. In fact not all dihedral angles change drastically during complex formation as can be seen for SC1C2N and C3C4C5O dihedral angles in Table 5, which do not change much during complex formation. This indicates that bond rotation is critical for complex formation. There are great similarities in all structural parameters between Ni and Cu complexes.

Trivalent metal complexes. The C1—C2, C3—C4, C4—C5 and C6—C6′ bond lengths have slight changes during complexation process in the range of 0.03 Å. This is a similar finding as divalent metal complexes and indicates the effect of complex on geometrical parameters is still mainly localized near to the ligating atoms. The M—N and M—O bond lengths are shorter for Cr complex than Fe complex while M—S bond length is shorter for Fe complex than Cr complex. This shows more affinity for Fe to interact with S containing ligand than Cr. The M—O of Cr complex is shorter than all divalent metal complexes. This shows more affinity for Cr to interact with O containing ligand. Both Fe(III) and Mn(II) metals has $3d^5$ electronic configuration with larger charge on Fe metal. This explains why M—N, M—O and M—S bond lengths in case of Fe complex are shorter than Mn complex.

The S—C1, N—C2, O—C5 and O—C6 bond lengths for Cr complex is longer than both Fe complex and all divalent metal complexes. The N—C3 bond length for Cr and Fe complexes are equal, but longer than N—C3 bond length for all divalent metal complexes. This indicates a greater interaction with trivalent metal than divalent ones.

The SMO′, SMN′, NMO and NMO′ bond angles of Cr complex is larger than that of Fe complex while the SMO and SMN bond angles of Cr complex are smaller than that of Fe complex. The bond angles for Cr complex are similar to that of Ni complex. A similar trend for deviation of SMS′ and NMO′ bond angles, from regular octahedral were observed as in case of divalent metal. SMS′ and NMO′ bond angles for Cr complex are larger than Fe complex by about 20°. This indicates Cr complex is more near to regular octahedral than Fe complex.

The dihedral angle NC3C4C5 and OC6C6′O′ is similar in Cr and Fe complexes but smaller than in all divalent metal complexes.

Thorium complex. The tetravalent group in this paper contains one metal complex which is thorium metal complex. The C1—C2, C3—C4, C4—C5 and C6—C6′ bond lengths have slight changes during complexation process in the range of 0.01 Å. This is a similar finding as divalent and trivalent metal complexes and indicates the effect of complex on geometrical parameters which are still mainly localized near to the ligating atoms. The M—N bond length is larger than divalent and trivalent metal complexes. The M—O and M—S bond lengths are long and come in order, after Zn and Cu complexes, respectively. This can be explained by the larger size of the Th(IV) metal ion compared to 3d metal ions. The S—C1, N—C2, N—C3, O—C5 and O—C6 bond lengths are longer than divalent and trivalent metal complexes. The S—C1, N—C2, N—C3 and O—C5 bond lengths of all complexes show a general trend of elongation compared to synclinal L^{2-} with maximum elongation in case of Th complex. This elongation indicates a stronger bond between Th and ligand.

The deviation from regular octahedral in Th complex can be detected by the deviation of SMO and NMN′ bond angles from 180° since they are the largest two angles in this complex. This indicates a quiet change in geometry compared to divalent and trivalent metal complexes. NMN′ bond angle is less deviated than SMO bond angle from regular octahedral.

The dihedral angle OC6C6′O′ in Th complex is 48° which is very different compared to divalent and trivalent metal complexes which vary between 57° and 65° These geometrical data suggest that complex formation involves more bond rotations rather than bond elongation or shorting which is summarized in Table 5.

Energetics and Mulliken atomic charges for the complexes

The energetics of the complexes are shown in Table 6. The existence of multiplicity higher than 1 indicates the presence of weak field ligand. The multiplicity higher than 1 results in splitting of HOMO and LUMO into different spins namely alpha and beta. The energy difference ΔE for complexes are all in range of 2.5 eV with exception for Cu complex which has 1.4 eV. The lower ΔE usually indicates higher reactivity [43,44]. This means that Cu complex is more reactive than all other complexes. The atomic charges are shown in Table 6. The donor atoms total charges are almost unchanged (in case of Co complex) or slightly increase (in case of Mn, Fe, Ni and Cu complexes) or slightly decrease (in case of Zn, Cr and Th complexes) during complexation. The increase in donor charge suggests a back-donation from metal to ligand. The remaining charges, (which are the summation of charges on all atoms other than donating atoms on the ligand) are more positive suggesting electrons moves from many atoms in the ligand to metal during complexation due to hyperconjugation.

The $E_{binding}$ is the energy difference between the complex and summation of the energy of metal ion and synclinal L^{2-}. The $E_{binding}$ indicate the total energy released during the formation of metal–ligand bonds. As charge on metal increase the $E_{binding}$ increase with maximum for Th complex. Among divalent metals the highest $E_{binding}$ is for Ni complex and the smallest $E_{binding}$ is

Table 6
The energetic and Mulliken atomic charges of the synclinal L^{2-} and its complexes.

	L^{2-}(synclinal)	[Mn(L)]	[Co(L)]·H_2O	[Ni(L)]·H_2O	[Cu(L)]·$2H_2O$	[Zn(L)]	[Cr(L)]Cl	[Fe(L(]Cl	[Th(L)]·Cl_2
E total, a.u	−2136.5477	−3287.5635	−3519.2583	−3644.7640	−3776.8574	−3915.7463	−3180.8661	−3400.0318	−651.5303
α_{LUMO}, eV	3.6953	−1.8123	−1.8259	−1.7796	−1.9048	−1.7633	−5.0750	−4.9335	−8.4274
β_{LUMO}, eV		−1.8613	−1.8912	−1.7932	−2.8436		−5.3090	−6.1444	
α_{HOMO}, eV	1.2653	−4.4518	−4.4681	−4.4028	−4.3511	−4.5960	−7.8587	−8.1063	−11.2302
β_{HOMO}, eV		−4.5960	−4.4790	−4.4001	−4.2831		−7.8886	−8.1716	
ΔE, eV	2.4300	2.5905	2.5769	2.6069	1.4395	2.8327	2.5497	1.9619	2.8028
M-charge		+0.963524	+0.720089	+0.731320	+0.783379	+0.662755	+0.848336	+1.063905	+1.202559
Total charge	−2.0	0.0	0.0	0.0	0.0	0.0	+1.0	+1.0	+2.0
O-charge	−0.485846	−0.576293	−0.555079	−0.569756	−0.581049	−0.546835	−0.622796	−0.613919	−0.942895
N-charge	−0.386123	−0.568584	−0.550947	−0.536275	−0.532022	−0.509583	−0.573052	−0.624039	−0.573711
S-charge	−0.561443	−0.411378	−0.314721	−0.349552	−0.396736	−0.297970	−0.181313	−0.236790	+0.221613
Donors-charge	−2.866824	−3.11252	−2.8415	−2.91116	−3.01962	−2.70878	−2.754322	−2.9495	−2.58998
Remaining	+0.866824	+2.149	+2.12141	+2.17984	+2.23624	+2.04603	+2.905986	+2.8856	+3.387421
μ(debye)	4.147	6.7082	6.7610	4.9191	5.2063	6.1185	4.6373	4.5427	12.0558
Multiplicity	1	6	4	3	2	1	4	6	1
$E_{binding}$(kcal/mol)		622.82	678.76	697.80	688.14	685.03	1293.31	1249.36	1441.12

for Mn complex. For trivalent metals, the $E_{binding}$ for Cr complex is higher than for Fe complex.

Conclusion

The eight new metal complexes of novel Schiff base with Cr(III), Mn(II), Fe(III), Co(II), Ni(II), Cu(II), Zn(II) and Th(IV) were prepared and isolated as solids and formulated as [ML]·xH_2O (M = Mn(II) (x = 0), Co(II) (x = 1), Ni(II), (x = 1), Cu(II) (x = 2) and Zn(II) (x = 0)) and [ML]·nCl (M = Cr(III) (n = 1), Fe(III) (n = 1) and Th(IV) (n = 2)). The complexes have been characterized using melting point, molar conductance, magnetic properties, elemental analysis, IR, molar conductance, ^{1}H NMR and thermal analyses. From these techniques, it may observed that the azomethine, thiophenolic SH and etheric O groups in all complexes shifted to lower values in IR spectra support the chelation effect via these groups. Also, the nondetectable of signals for thiophenolic proton in the ^{1}H NMR spectra of the complexes support the chelation of thiophenolic SH. The complexes are found to have octahedral geometry according to the data of magnetic moment and diffused reflectance spectra.

The DFT calculations for the ligand show that free rotation around aliphatic CH_2- CH_2 has the main role during complex formation. The bond length elongation and shortening are localized near to the metal in complex and main geometrical changes are mainly in both bond angles and dihedral angles. The complexes show multiplicity higher than 1 which means the ligand has weak field ligand. Among divalent metal complexes Cu is more reactive than other complexes. The binding energy for Ni Complex is highest among divalent metal complexes followed by Cu complex. The binding energy for Cr complex is higher than Fe complex. Charges on ligating atoms suggest a back-donation from ligand to metal specially for Mn, Fe, Ni and Cu complexes. Calculations results are in good agreement with experimental values and assess more conformation details than experimental data that recommends the need for computational data to explain the complicated structures of inorganic complexes.

References

[1] Sima, Craot, Chem. Acta 74 (2001) 593–600.
[2] N.V. Tverdova, E.D. Pelevina, N.I. Giricheva, G.V. Girichev, N.P. Kuzmina, O.V. Kotova, J. Mol. Struct. 1012 (2012) 151–161.
[3] C. Anitha, C.D. Sheela, P. Tharmaraj, S. Sumathi, Spectrochim. Acta (Part A) 96 (2012) 493–500.
[4] N. Raman, S. Sobha, A. Thamaraichelvan, Spectrochim. Acta (Part A) 78 (2011) 888–898.
[5] Abdel-Nasser M.A. Alaghaz, Badr A. El-Sayed, Ahmed A. El-Henawy, Reda A.A. Ammar, J. Mol. Struct. (103) (2013) 83–93.
[6] M.B. Halli, R.B. Sumathi, Mallikarjun Kinni, Spectrochim. Acta (Part A) 99 (2012) 46–56.
[7] Madhavan Sivasankaran Nair, Dasan Arish, Raphael Selwin Joseyphus, J. Saudi Chem. Soc. 16 (2012) 83–88.
[8] S. Sobha, R. Mahalakshmi, N. Raman, Spectrochim. Acta (Part A) 92 (2012) 175–183.
[9] Azza A.A. Abou-Hussein, Wolfgang Linert, Spectrochim. Acta (Part A) 95 (2012) 596–609.
[10] A.D. Tiwari, A.K. Mishra, S.B. Mishra, B.B. Mamba, B. Maji, S. Bhattacharya, Spectrochim. Acta (Part A) 79 (2011) 1050–1056.
[11] Bibhesh K. Singh, Hemant K. Rajour, Anant Prakash, Spectrochim. Acta (Part A) 94 (2012) 143–151.
[12] A.D. Garnovskii, I.S. Vasil Chenko, Russ. Chem. Rev. 71 (2002) 943–996.
[13] A.D. Garnovskii, A.L. Nivorozhkin, V.I. Minkin, Coord. Chem. Rev. 126 (1993) 367–370.
[14] S.B. Desai, P.B. Desai, K.R. Desai, Hetrocycl. Commun. 7 (2001) 83–90.
[15] P.V. Pathak, S. Jolly, K.P. Sharma, Orient. J. Chem. 16 (2000) 161–167.
[16] A. Halve, S. Samadhiya, Orient. J. Chem. 17 (2001) 87–88.
[17] O.A. Weber, T.W. Robinson, V.I. Simeon, J. Inorg. Nucl. Chem. 33 (1971) 2097–2101.
[18] N. Manav, N. Gandhi, N.K. Kaushik, J. Therm. Anal. Calorim. 61 (2000) 117–127.
[19] N.K. Singh, A. Srivastava, A. Sodhi, P. Ranfan, Trans. Met. Chem. 25 (2000) 133–140.
[20] N.H. Patel, H.M. Parekh, M.N. Patel, Trans. Met. Chem. 30 (2005) 11–13.
[21] Y.P. Tian, C.Y. Duan, C.Y. Zho, X.Z. You, T.C.W. Mak, Z. Zhang, Inorg. Chem. 46 (2007) 4660–4666.
[22] X.Y. Cao, M. Dolg, J. Mol. Struct. (Theochem.) 581 (2002) 139–147.
[23] T. Schaefer, T.A. Wildman, R.H. Salman, J. Am. Chem. Soc. 102 (1980) 102–107.
[24] T. Schaefer, S.R. Salman, T.A. Wildman, P.D. Clark, Can. J. Chem. 60 (1982) 342–348.
[25] J.D. David, H.E. Hallam, Spectrochim. Acta (Part A) 21 (1965) 841–848.
[26] A.D. Becke, J. Chem. Phys. 98 (1993) 5648–5652.
[27] J.M. Martin, J. El-Yazal, J. Francois, Mol. Phys. 86 (1995) 1437–1450.
[28] M.J. Frisch, G.W. Trucks, H.B. Schlegel, G.E. Scuseria, M.A. Robb, J.R. Cheeseman, G. Scalmani, V. Barone, B. Mennucci, G.A. Petersson, H. Nakatsuji, M. Caricato, X. Li, H.P. Hratchian, A.F. Izmaylov, J. Bloino, G. Zheng, J.L. Sonnenberg, M. Hada, M. Ehara, K. Toyota, R. Fukuda, J. Hasegawa, M. Ishida, T. Nakajima, Y. Honda, O. Kitao, H. Nakai, T. Vreven, J.A. Montgomery Jr., J.E. Peralta, F. Ogliaro, M. Bearpark, J.J. Heyd, E. Brothers, K.N. Kudin; V.N. Staroverov; R. Kobayashi; J. Normand; K. Raghavachari; A. Rendell; J.C. Burant; S.S. Iyengar; J. Tomasi; M. Cossi; N. Rega; J.M. Millam; M. Klene; J.E. Knox; J.B. Cross; V. Bakken; C. Adamo; J. Jaramillo; R. Gomperts; R.E. Stratmann; O. Yazyev; A.J. Austin; R. Cammi; C. Pomelli; J.W. Ochterski; R.L. Martin; K. Morokuma; V.G. Zakrzewski; G.A. Voth; P. Salvador; J.J. Dannenberg; S. Dapprich; A.D. Daniels; O. Farkas; J.B. Foresman; J.V. Ortiz; J. Cioslowski; D.J. Fox; Gaussian, Inc., Wallingford CT, 2009.
[29] http://www.chemcraftprog.com.
[30] S. Ilhan, H. Temel, I. Yilmaz, M. Sekerci, J. Organom. Chem. 692 (2007) 3855–3865.
[31] Hanan F. Abd Elhalim, M.M. Omar, Gehad G. Mohamed, Mohsen Abou El-Ela Sayed, Eur. J. Chem. 2 (2011) 178–188.
[32] Mostafa M.H. Khalil, Eman H. Ismail, Gehad G. Mohamed, Ehab M. Zayed, Ahmed Badr, Open J. Inorg. Chem. 2 (2012) 13–21.
[33] Farag M.A. Altalbawy, Gehad G. Mohamed, Mohsen Abou El-Ela Sayed, Mohamed I.A. Mohamed, Monat. Chem. – Chem. Month. 143 (2012) 79–89.
[34] F.A. Cotton, G. Wilkinson, C.A. Murillo, M. Bochmann, Advanced Inorganic Chemistry, sixth ed., Wiley, New York, 1999. pp. 848–867.
[35] G.G. Mohamed, N.E. El-Gamel, Vib. Spectrosc. 36 (2004) 97–104.
[36] M.M. Omar, Gehad G. Mohamed, Amr A. Ibrahim, Spectrochem. Acta (Part A) 73 (2009) 358–369.
[37] G.G. Mohamed, M.M. Omar, Amr A. Ibrahim, Eur. J. Med. Chem. 44 (2009) 4801–4812.
[38] G.G. Mohamed, Sayed M. Abdallah, M.A. Zayed, M.M.I. Nassar, Spectrochim. Acta (Part A) 74 (2009) 635–641.
[39] S.M. Abdallah, G.G. Mohamed, M.A. Zayed, M. Abu Elela, Spectrochim. Acta (Part A) 73 (2009) 833–840.
[40] Hanan F. Abd El-Halim, Gehad G. Mohamed, Maher M.I. El-Dessouky, Walaa H. Mahmoud, Spectrochim. Acta, (Part A) 82 (2011) 8–19.
[41] M.H. Soliman, Gehad G. Mohamed, Spectrochim. Acta (Part A) 91 (2012) 11–17.
[42] H-Y. Zhang, H-F. Ji, J. Mol. Struct. (Theochem.) 663 (2003) 167–174.
[43] L. Herrag, B. Hammouti, S. Elkadiri, A. Aouniti, C. Jama, H. Vezin, F. Bentiss, Corros. Sci. 52 (2010) 3042–3051.
[44] I.B. Obot, N.O. Obi-Egbedi, Corros. Sci. 52 (2010) 198–204.